Absorption and Fluorescence Studies of Acridine in Subcritical and Supercritical Water

E. Todd Ryan, Tao Xiang, Keith P. Johnston,* and Marye Anne Fox*

Departments of Chemistry and Biochemistry and of Chemical Engineering, The University of Texas at Austin, Austin, Texas 78712

Received: August 30, 1996; In Final Form: November 7, 1996[⊗]

The isobaric acid/base equilibrium between acridine and the acridinium cation was measured from ambient temperature to 380 °C (above the critical temperature of water, $T_c = 374$ °C) using absorption spectroscopy. At 3500 psia, the isobaric protonation of acridine is shown to be exothermic up to approximately 315 °C. Above 315 °C, protonation becomes endothermic due to changes in the dielectric constant of water with temperature, which has a profound influence on the solvation of ions. The results are interpreted using a modified Born equation to account for the temperature-dependent changes in acridinium cation and proton solvation. The absorption and fluorescence spectra and the fluorescence lifetime of acridine are sensitive to changes in solvent−solute hydrogen bonding. Hydrogen bonding between acridine and water is observed to decrease from ambient temperature to the critical temperature. A relatively rapid change in hydrogen bonding occurs between 100 and 200 °C.

Introduction

Water is the most important solvent in nature. It is unique largely because a single water molecule can form up to four strong hydrogen bonds.[1,2] These play a major role in solvation and cause water, unlike other solvents, to expand upon freezing. Because water is the medium of life, studies of its liquid-, solid-, and gas-phase properties began centuries ago and continue today.[3] Recently, the unusual properties of supercritical water (SCW) have attracted much scientific study primarily because of SCW's potential in many industrial processes and for environmental remediation.[4−7] Some examples include hydrothermal oxidation of organic wastes, hydrothermal breeding of crystals, spraying of ceramics, and hydrothermal synthesis such as the hydrolysis of chlorobenzene to form phenol and dibenzofuran.[8]

The objective of this study is to characterize the thermodynamics of the acid−base equilibrium (eq 1) and the photophysics

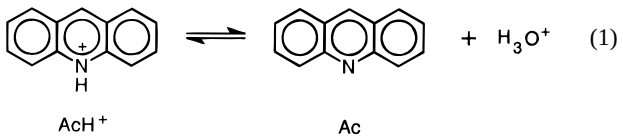

(1)

of acridine in subcritical and SCW. The effects of ion solvation on the acid−base equilibrium (eq 1) are accounted for using a modification of the Born equation, and the results are compared with experimental results for the reactions of OH^- with 2-naphthol[9] and 2-naphthoic acid[10] and calculational studies (continuum electrostatic, CE, and molecular dynamic-free energy perturbation, MD-FEP) simulations of the reaction of HCl and OH^-.[11,12] In addition, the temperature dependence of the acridine fluorescence and absorption spectra are consistent with a marked decrease in intermolecular hydrogen-bond interactions. These results indicate that the hydrogen-bond network of water dissipates above 100 °C at 3500 psia.

Widespread interest in SCW as a reaction medium has sparked a growing research effort to understand SCWs unique solvation properties. The structure of SCW solutions has been probed with molecular dynamics computational simulation.[17,18] MD-FEP simulation is a powerful tool to relate the solvation free energy of neutral and ionic species to solvation structure at a molecular level.[11,19−22] However, MD-FEP simulation is limited by the large amount of computer time required. Continuum electrostatic (CE) models for the solvation free energy, which are numerical solutions to Poisson's equation, require far less computer time. CE models predict the free energies of solvation for various neutral and ionized species in ambient water quite accurately,[23] and this allows other properties such as relative acidities, reaction rates, and equilibrium constants to be determined from classical thermodynamics. The results of CE and MD-FEP models for the S_N2 reaction of Cl^- with CH_3Cl have been compared recently.[24] The simulated free energy for the pentavalent transition state, $Cl^{\delta-}\cdots CH_3\cdots Cl^{\delta-}$, was accurately predicted with a CE model at low and high densities relative to the critical density. However, the model failed in the middensity region where electrostriction is most prevalent. In contrast, a CE model did accurately predict the acidity of HCl relative to water, $HCl + OH^- = Cl^- + H_2O$, at all densities studied.[12] This reaction does not generate charge (isocoulombic), and the reactant and product ions are about the same size. Thus, the errors which result from neglecting electrostriction cancel.

Recently, the effects of pressure and temperature on the equilibrium constant, K_{BHA}, for the reaction of 2-naphthol (2-NpOH) with OH^- [9] and of 2-naphthoic acid with NH_3[10] were studied in subcritical and SCW. The Born model was used to account for changes in ionic solvation with temperature, pressure, and density. At constant temperature, density had a much greater effect on the acid dissociation constant, K_a, of 2-NpOH than on K_{BHA} because the former reaction produces a pair of positive and negative ions, i.e., is ionogenic, whereas the latter converts one anion to another with no net change in number or charge of ions. At constant density, the temperature dependence of K_{BHA} indicates that the isocoulombic reaction of 2-NpOH and OH^- is exothermic but that of K_a indicates that the ionization of 2-NpOH is endothermic, presumably because the energy required for ionization is greater than the solvation energy gained by the products 2-NpO^- and H^+. At constant pressure, more complex behavior is observed because the large partial molar enthalpies, entropies, and volumes of ions all

[⊗] Abstract published in *Advance ACS Abstracts,* February 1, 1997.

S1089-5639(96)02676-X CCC: $14.00

change with temperature as a result of water's large isothermal compressibility and volume expansivity.

Many of water's unique properties are due to strong hydrogen-bonding interactions which give liquid water a propensity to maintain a tetrahedral structure.[1,25,26] For example, rotational correlation phenomena such as dielectric relaxation and shear viscosity depend on cooperative hydrogen-bond interactions among water molecules. Robinson and co-workers have suggested that proton- and electron-transfer reactions to water are also dependent on cooperative hydrogen bonding, and they found the rate of excited-state deprotonation of 2-naphthol by water to be proportional to the Debye relaxation time up to 80 °C.[27] Like other rotational correlation phenomena, the Debye relaxation time of water depends upon the rotational motions of clustered water molecules that are hindered by water's extensive hydrogen-bond network.

Green and co-workers studied excited-state deprotonation of 2-naphthol up to 400 °C.[13] Their results were consistent with those of Robinson up to 80 °C where the proton-transfer rate followed linear Arrhenius behavior. Above 100 °C, however, the proton-transfer rate was non-Arrhenius and much slower than expected based on an Arrhenius extrapolation from the low-temperature data. They concluded that changes in water structure above 100 °C prevented water from solvating the proton. Ryan and co-workers studied excited-state deprotonations of 2-naphthol to water and several bases to 400 °C and observed a qualitative difference between the temperature dependence of ionogenic and isocoulombic reactions.[28] Excited-state deprotonations of 2-naphthol by water and ammonia are ionogenic and exhibit non-Arrhenius behavior similar to that observed by Green and co-workers. The transition states of ionogenic reactions are desolvated relative to the reactants as the temperature is increased. This, in turn, alters the activation free energy, and the ionogenic proton-transfer rates become non-Arrhenius. Deprotonations by acetate and borate anions are isocoulombic and are nearly Arrhenius-like up to the critical temperature. The transition states of isocoulombic proton-transfer reactions have the same charge as the reactants and are not significantly desolvated relative to the reactants in high temperature water. Thus, the activation free energy varies only modestly with temperature. Pronounced deviations from Arrhenius behavior are observed for the ionogenic reactions above 100 °C and are consistent with a large change in hydrogen-bond interactions above this temperature.

Consistent with this are the results of a molecular dynamics simulation using the simple point charge extended (SPCE) model.[29] The simulation indicates that heating liquid water causes the hydrogen-bonded tetrahedral structure to dissipate. For example, the coordination number of pure saturated liquid water was shown to increase with temperature from 4.5 at 25 °C to about 5.9 by 200 °C. The tetrahedral structure of ambient water causes the coordination number to be about 4.5 instead of 12, which is expected for a simple Leonard-Jones liquid. At higher temperatures, the hydrogen-bond network dissipates, and the molecules in the first solvent shell become more free to reorient, making room for additional coordinated water molecules. Above 227 °C, the coordination number decreases as the bulk density decreases. Although hydrogen bond interactions markedly decrease between 100 and 200 °C, hydrogen bonding between two water molecules or in small clusters of water molecules can be observed to at least 527 °C.[30]

Experimental Section

Absorption spectra were obtained using a previously designed Inconel 625 high-pressure cell employing two sapphire windows (1 cm optical path length).[9] A second high-pressure cell, constructed from grade 2 Tico titanium fitted with three sapphire windows, was used to collect fluorescence spectra.[13] The choice of Ti was to avoid iron impurities. Pressure was monitored using a Heise Model 901A pressure indicator (0−10 000 psia). The temperature was monitored using a J-type thermocouple mounted in a 1.5 cm deep slot in the cell. An Omega Model CN76000 temperature controller was connected to heating tape, which was wrapped around the insulated cell. Resistive current was controlled with a variable transformer in conjunction with the temperature controller and maintained the cell temperature to within 1 °C. The sample solution was pumped into the cell using either an Eldex model AA-100-S HPLC pump (0−5000 psia) or a Beckman 1008 HPLC pump (0−6000 psia). Prior to use, all sample solutions were deaerated with nitrogen or He (Liquid Carbonic, 99.995%) which had been purified by passage through an oxygen trap (Alltech), effecting deaeration. After a 30 min purge, steady-state fluorescence was stable indefinitely.

Steady-state absorption spectra were collected using a Cary 3E absorption spectrometer. Steady-state fluorescence was recorded on an SLM Aminco 500 fluorimeter with the sample compartment modified to accept the high-pressure cell. Time-resolved data were collected by single-photon counting[14,15] at the Center for Fast Kinetics Research. All the steady-state and time-resolved data were collected using 350 or 355 nm as excitation wavelengths.

Acridine (Aldrich) was purified by recrystallization from ethanol and chromatography on neutral alumina with a 50% benzene/hexane mixture in a darkened room. The purity was checked by melting point (109−110 °C, lit.[16] 111 °C), high-resolution mass spectrometry, and high-resolution proton NMR. Sample solutions of acridine for fluorescence experiments (1×10^{-5} M) were prepared using ultrafiltered water (Millipore). The absorption experiments required a higher concentration of acridine (1×10^{-4} M). Fresh solutions were prepared each day, protected from light, and bubbled with He or N_2 to remove dissolved oxygen. Alternatively, a stock solution was prepared, protected from light, and stored under nitrogen. The pH of a 1×10^{-4} M aqueous acridine solution was ~6 at ambient temperature. The pH of the sample solutions was varied using HCl or KOH.

SCHEME 1: Illustration of the Relevant Photophysics of Acridine in Water

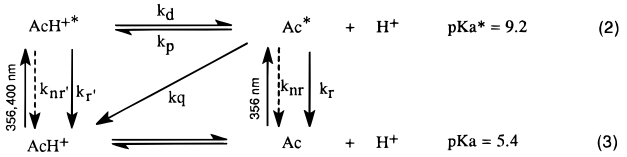

Results and Discussion

Absorbance Experiments. When acridine is excited to the S_1 π,π^* state, denoted here as Ac*, it becomes a much stronger proton acceptor. The pK_a of AcH^+ increases from pK_a = 5.4 to pK_a* = 9.2.[31] These processes are depicted in Scheme 1, which illustrates all of the relevant photophysics. The term "proton" and the symbol, H^+, are used throughout this paper to represent the solvated proton. The notation is a generic representation and makes no claim on the nature of proton solvation, which undoubtedly involves local aggregation. In a neutral aqueous solution at 25 °C with pH < pK_a*, Ac* is readily protonated (k_p, solvent-assisted proton transfer). Thus, in neutral water Ac* decays by solvent-assisted protonation with a rate constant, k_p, in competition with radiative (k_r) and

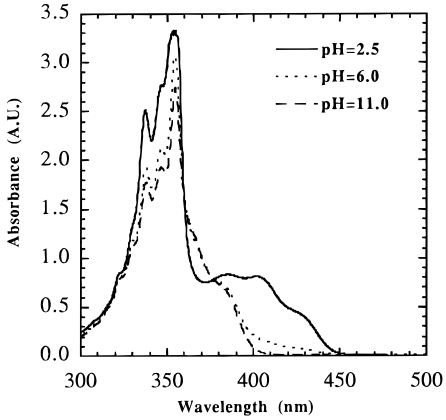

Figure 1. Absorption spectra of acridine (1×10^{-4} M) in deaerated water at room temperature and pressure at three pH values: 2.5, 6, and 11. The maximum absorbance of each spectrum is normalized to one.

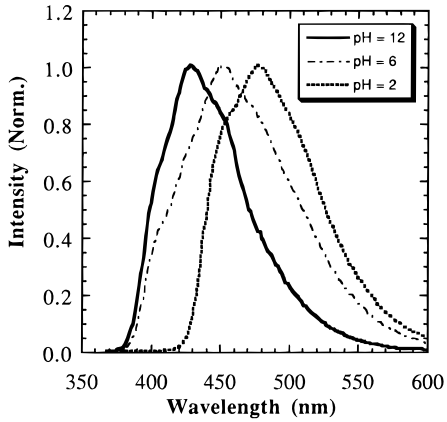

Figure 2. Steady-state fluorescence spectra of acridine (1×10^{-4} M) in deaerated water at room temperature and pressure at three pH values: 2, 6, and 12. The maximum fluorescence of each spectrum is normalized to one.

nonradiative (k_{nr}) relaxation. Protonation forms the acridinium cation in its S_1 state (AcH^{+}*), and it decays with its own characteristic radiative (k_r') and nonradiative (k_{nr}') pathways.

The absorption maxima of both AcH^+ and Ac appear at 356 nm, but the AcH^+ spectrum has a broad shoulder centered at approximately 400 nm that is not present in the Ac absorption spectrum (Figure 1). The shoulder is sufficiently resolved from the main peak to allow absorption spectroscopy to monitor the concentrations of AcH^+ and Ac. Thus, steady-state absorption spectroscopy probes the ground-state equilibrium behavior of aqueous acridine.

The fluorescence maximum of Ac* appears at approximately 430 nm, whereas that of AcH^{+}* appears at approximately 475 nm (Figure 2). Protonation is favored when the pH of the reaction mixture is lower than that of the reaction's pK. When the pH < pK_a, AcH^+ is the predominant species, and excitation of AcH^+ to AcH^{+}* does not result in excited-state deprotonation because pH $\ll$ pK_a*. Thus fluorescence from AcH^{+}* only is observed. When pK_a < pH < pK_a*, Ac is the predominant species present and excitation of Ac to Ac* results in excited-state protonation while excitation of AcH^+ to AcH^{+}* does not induce excited-state deprotonation. In this case, fluorescence is observed from both Ac* and AcH^{+}* (middle spectrum in Figure 2). Only Ac is present if the pK_a < pH, and excitation to Ac* generates fluorescence from that species only (λ_{max} = 475 nm, spectrum in Figure 2).

Acid/Base Equilibrium. Steady-state absorption spectroscopy is used to determine the isobaric temperature dependence

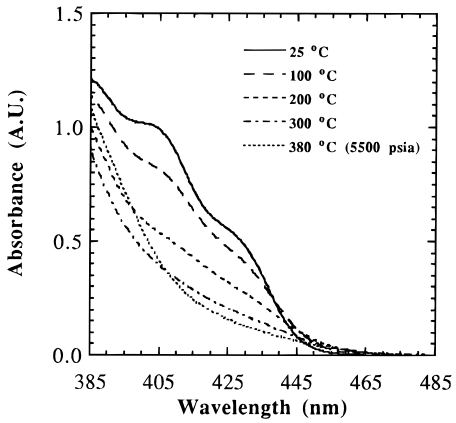

Figure 3. Absorption spectra of acridine (1×10^{-4} M) in deaerated water adjusted to pH 3.9 at several temperatures at 3000 psia normalized to water density at ambient temperature. The spectral region shown is that where AcH^+ does not significantly overlap with Ac. The data at 380 °C were obtained at 5500 psia to avoid a phase transition.

of the ground-state acid−base equilibrium between acridine and the acridinium cation (eq 3). The absorption spectra of aqueous solutions of acridine (pH 3.9) at several temperatures at 3500 psia are shown in Figure 3. Only the 385−485 nm region is displayed because AcH^+ is the primary absorber in this wavelength region. As the temperature is increased, the AcH^+ concentration decreases until the AcH^+ absorption (λ_{max} = 405 nm) disappears. The loss of AcH^+ indicates the reaction is shifting toward Ac as the temperature is increased. The exothermic behavior for the protonation reaction is expected below the critical temperature, since the proton is a much stronger acid than AcH^+ in subcritical water. The AcH^+ concentration also decreases with temperature in a pH 2.1 aqueous solution of acridine, but the change is not as large as that observed in the pH 3.9 solution because the higher proton concentration favors AcH^+. While AcH^+ absorption nearly disappears by 300 °C in the pH 3.9 solution, the acridinium cation absorption is present up to 380 °C in a more acidic solution.

The temperature dependence of the acridine acid−base equilibrium (eq 3) is quantified by measuring the equilibrium constant at constant pressure as a function of temperature. This is accomplished using steady-state absorption spectroscopy to determine the concentrations of Ac and AcH^+ as described below. The reaction of acridine with water is written as

$$Ac + H_2O = AcH^+ + OH^- \quad (4)$$

where the equilibrium constant is

$$K_b = m_{AcH^+} m_{OH^-}/m_{Ac} \quad (5)$$

and the infinite dilution activity coefficient of each species and the mole fraction of water (symbols not shown in the equation) are defined as unity. For the deprotonation of a neutral acid, HA such as 2-naphthol with OH^-, the corresponding equilibrium constant is often referred to as K_{BHA}. For the ionization of water

$$H_2O = H^+ + OH^- \quad (6)$$

the ionization equilibrium constant is expressed as

$$K_w = m_{H^+} m_{OH^-} \quad (7)$$

As in eq 5, the mole fraction of water and the activity coefficients are assumed to be unity. The reaction of acridine with H^+ (eq 8) is obtained by subtracting eq 6 from eq 4:

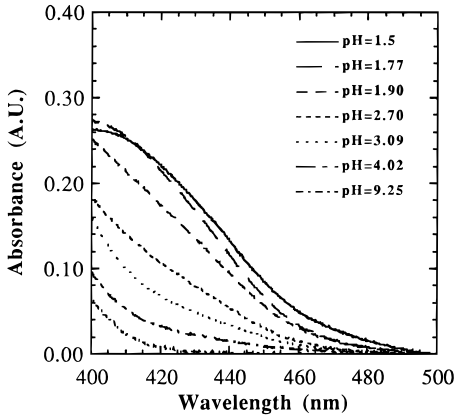

Figure 4. Absorption spectra of AcH^+ in deaerated aqueous acridine solutions (1×10^{-4} M) at several pH values at 350 °C and 3500 psia normalized to the water density at ambient temperature.

$$Ac + H^+ = AcH^+ \tag{8}$$

and the equilibrium constant for eq 8 is

$$K_a^{-1} = K_b/K_w = m_{AcH^+}/m_{Ac}m_{H^+} \tag{9}$$

Thus, K_a^{-1} is a relative property relating the basicity of acridine to that of water. Rearranging eq 9 gives

$$\log(m_{Ac}/m_{AcH^+}) = -\log K_a^{-1} - \log [H^+] \tag{10}$$

from which K_a^{-1} is determined from m_{Ac}/m_{AcH^+} and $[H^+]$ at a given temperature. The ratio m_{Ac}/m_{AcH^+} is obtained from the AcH^+ absorbance integrated from 400 to 500 nm. The absorbance of AcH^+ was not integrated below 400 nm because of significant spectral overlap with the unprotonated acridine absorbance. The AcH^+ absorbance was deconvoluted from the small spectral overlap of Ac as described previously.[9] From 25 to 400 °C, acridine in pH 1.5 solution is assumed to be completely protonated since the absorption spectrum does not change when the pH is decreased further. Thus, in pH 1.5 solutions, the integrated absorbance of acridine corresponds to the absolute AcH^+ concentration, which is equal to the initial acridine concentration, providing a calibration between AcH^+ absorbance and concentration from 25 to 400 °C. Because the concentration of Ac can be calculated from $[AcH^+]$ by mass balance, the ratio m_{Ac}/m_{AcH^+} is determined from the integrated AcH^+ absorbance alone.

At each temperature studied, e.g., at 350 °C as shown in Figure 4, the absorption spectra are obtained in solutions of varying initial pH in order to determine K_a from eq 10. The pH is adjusted using HCl, so the proton concentration must be corrected for the temperature dependence of the HCl acid−base equilibrium using the equation of Mesmer.[32] All experiments were performed under conditions such that the values of $\log(m_{Ac}/m_{AcH^+})$ ranged from 1 to −1. Outside of this range, the results are sensitive to small errors in the absorbance data. Figure 5 displays data obtained at three temperatures plotted according to eq 10. Similar plots constructed for each temperature studied were all linear with a slope of 1 as expected from eq 10. The values of K_a^{-1} are determined from the intercepts of these plots and are plotted in Figure 6 for a pressure of 241 bar. In regions where acridine was stable, the reproducibility in the logarithm of the concentration ratio in Figure 5 was ±0.1 log units at temperatures below 380 °C and ±0.2 log units at 380 °C. Based on eq 10, the reproducibilities for $\log K_a^{-1}$ are comparable, assuming that the reproducibilities in pH for the HCl data are similar to this. Finally, the deviations from linearity in Figure 5 are within the experimental uncertainty and do not reflect curvature in the plot. For comparison, the figure also displays data measured along the saturation curve by Huh and co-workers.[33]

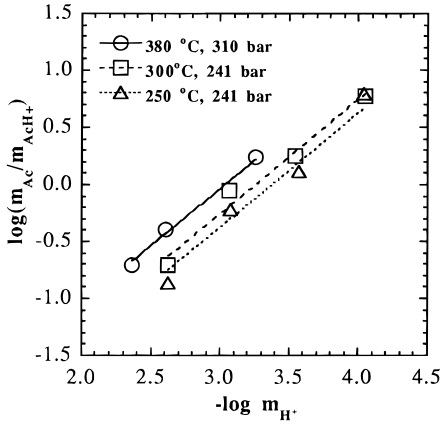

Figure 5. Dependence of the ratio of neutral and protonated acridine on solution pH at 3500 psia and several temperatures: 380 °C (circles), 300 °C (squares), and 250 °C (triangles). Above ambient temperature, the proton concentration was calculated from the pH at ambient temperature and the known temperature dependence of the HCl acid/base equilibrium.[32] The experimental uncertainty is ±0.1 log units at temperatures below 380 °C and ±0.2 log units at 380 °C.

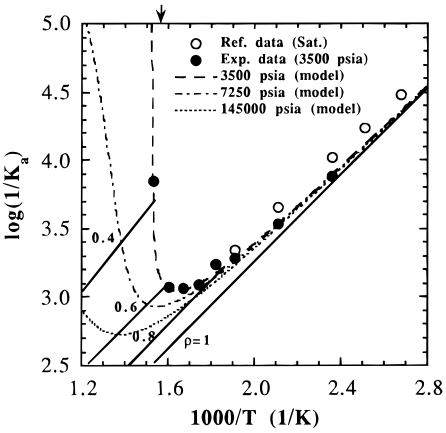

Figure 6. Dependence of K_a^{-1} for aqueous acridine on temperature observed at 3500 psia (solid circles). These experimental data are compared with that obtained along the saturation curve by Huh and co-workers[33] (open circles): the dashed lines represent the temperature dependence predicted by the modified Born equation at several pressures. The 3500 psia dashed solid line is the best fit to our data using the modified Born equation. The solid lines represent constant density in units of g/mL.

Shifts in the temperature and density of water can significantly affect acid−base equilibria because of changes in the value of ΔH, the temperature and density dependence on the dielectric constant, and electrostriction of water around ions.[9] For example, the equilibrium constant for the ionization of water, K_w (an ionogenic process), changes by about 5 orders of magnitude between 25 and 374 °C, and ϵ varies from ∼80 in ambient water to <10 in supercritical water.[34] Unlike neutral species, the solvation energies of ions are strongly dependent on ϵ: therefore, the equilibrium constants of ionogenic reactions are substantially altered by changes in ϵ, and the solvation of product ions relative to the neutral reactants largely determines the observed temperature dependence. In contrast, isocoulombic equilibria depend much less on ϵ because the ion solvation of the products and reactants is similar.

A modification of the Born equation, eq 11, that was used successfully to describe the temperature and density dependence

of ionogenic and isocoulombic acid−base reactions of 2-naphthol[9] was used here to describe the temperature dependence of K_a^{-1}:

$$\ln K_a^{-1} = -\frac{\Delta G°(T,\rho)}{RT} = \frac{\Delta G°(T_0,\rho_0)}{RT_0} + \left(\frac{\partial \ln K_a^{-1}}{\partial(1/T)}\right)_{\rho_0}\left(\frac{1}{T}-\frac{1}{T_0}\right) + \frac{83549}{T}\left(\frac{1}{\epsilon}-\frac{1}{\epsilon_0}\right)\left(\frac{1}{R^*_{H^+}}-\frac{1}{R^*_{AcH^+}}\right) \quad (11)$$

where $\epsilon_0 = \epsilon_0(\rho_0,T)$. For comparison, Figure 6 compares our experimental data with data collected along the saturation curve reported by Huh and co-workers[33] and with calculated behaviors. The first term in eq 11, $\Delta G°(T_0,\rho_0)$, is evaluated from the pK_a of acridine at 25 °C. The temperature derivative in the second term of eq 11 is determined from the data obtained below 200 °C because density is approximately constant (∼10% change) over this temperature range. The dielectric constant in the third term was calculated from the density using an equation given by Uematsu and Frank.[35] The density was calculated with an equation of state given with the steam tables reported by Haar.[36] The last term in eq 11, the Born term, requires estimations of the radii for the solvated proton, $R^*_{H^+}$, and the acridinium cation, $R^*_{AcH^+}$. Because $R^*_{H^+}$ is not known accurately, the value of $1/R^*_{H^+} - 1/R^*_{AcH^+}$ was determined by fitting eq 11 to the experimental data in Figure 6, giving a value of 0.19 A^{-1}. A positive value for $1/R^*_{H^+} - 1/R^*_{AcH^+}$ implies that AcH^+ is a larger ion than the proton as expected. The 3500 psia line in Figure 6 corresponds to the best fit of eq 11 to the data where $1/R^*_{H^+} - 1/R^*_{AcH^+}$ is the only adjustable parameter. If it were assumed that AcH^+ is much larger than the solvated proton, then $R^*_{H^+}$ would be on the order of the size of AcH^+. This analysis would suggest that the radii of both species contribute to the Born model. However, given the complexities of solvation in SCW and the simplicity of the Born model, the physical significance of the regressed value of $1/R^*_{H^+} - 1/R^*_{AcH^+}$ is quite limited.

Along the isobar at 3500 psia, K_a^{-1} decreases as the temperature is increased from ambient temperature to about 315 °C. This indicates that the protonation reaction, eq 8, is exothermic below 315 °C. In the range 315−350 °C, the temperature dependence of K_a^{-1} is much weaker, and K_a^{-1} abruptly increases near the critical temperature, indicating that the reaction changes from exothermic behavior in subcritical water to endothermic behavior in supercritical water. The equilibrium constants for other isocoulombic reactions exhibit similar behavior.[9] In subcritical water, the temperature dependence of the equilibrium constant is determined primarily by the second term in eq 11 because the difference between ϵ and ϵ_0 is relatively small, making the Born term small. At higher temperatures, where $\epsilon \ll \epsilon_0$, the significance of the Born term increases until it becomes dominant near the critical temperature. Thus, in supercritical water, the larger AcH^+ cation is favored when ϵ is small because of its smaller charge per volume. This induces the equilibrium shown in eq 8 to shift toward AcH^+, and the reaction exhibits endothermic behavior.

The dashed lines in Figure 6 are the values of K_a^{-1} predicted by eq 11 at different pressures using the same value of $1/R^*_{H^+} - 1/R^*_{AcH^+}$ determined from the fit to the 3500 psia data. At higher pressures, the difference between ϵ and ϵ_0 is not as great, and the Born term is less influential, even at the critical temperature. Therefore, the change from exothermic to endothermic behavior at pressures greater than 3500 psia is predicted to be less dramatic and shifted to higher temperatures. According to the model, much simpler behavior is observed at constant density, reflecting much smaller changes in the dielectric constant with temperature at constant density versus constant pressure. At constant density, log K_a^{-1} is fairly linear in temperature and always decreases with an increase in temperature, exhibiting exothermic behavior for protonation.

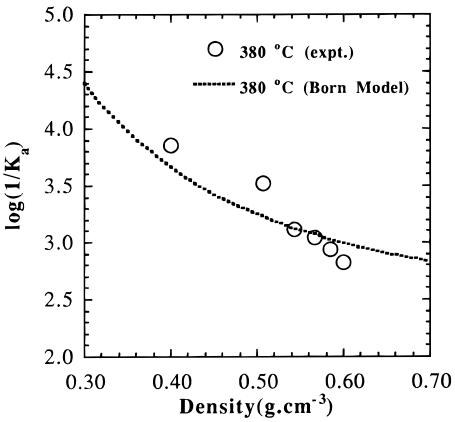

Figure 7. Dependence of K_a^{-1} for aqueous acridine on density at 380 °C. The dashed line is the density dependence of K_a^{-1} at 380 °C predicted by the modified Born equation. The experimental uncertainty is ±0.2 log units.

At 380 °C, the value of K_a^{-1} decreases as the bulk density is increased (Figure 7). This is consistent with the Born model, which predicts that the solvation of the proton relative to AcH^+ will increase as ϵ increases with density. This drives the equilibrium in eq 8 toward the reactants, and K_a^{-1} decreases. The dashed line in Figure 7 shows the change in K_a^{-1} predicted by eq 11, using $(1/R^*_{H^+} - 1/R^*_{AcH^+}) = 0.19$ Å^{-1}, as a function of density. It is not possible to determine the curvature of this plot from the data given for the experimental uncertainty at ±0.2 log units.

Essentially all of the results for the protonation of acridine in Figures 6 and 7 qualitatively match those for the deprotonation reactions: 2-naphthol + OH^- [9] and 2-naphthoic acid + OH^-.[10] At constant density both of these deprotonations are exothermic as a stronger acid and base react to a weaker acid and base. At constant pressure, each of these become endothermic in SCW as the loss in the dielectric constant with temperature favors the larger organic anion products versus OH^-, just as AcH^+ is favored over H^+. Together these three organic indicators may be utilized to measure the pH of SCW solutions over a wide range.

Fluorescence Experiments. We also attempted to study the temperature dependence of the excited-state acid/base equilibrium using steady-state fluorescence spectroscopy (Figure 8). In principle, fluorescence allows the determination of the relative concentrations of Ac* and AcH^+* and, therefore, the excited-state equilibrium constant. In pH 6 solutions of acridine, the fluorescence from both Ac* and AcH^+* is observed near room temperature. Protonation increases slightly when the temperature is raised to 200 °C because K_w increases about 2 orders of magnitude over this temperature range. The increased proton concentration drives the equilibrium toward protonation. The value of K_w decreases dramatically above 200 °C, lowering the proton concentration. This change in K_w drives the equilibrium toward the unprotonated species together with the equilibrium thermodynamics of an endothermic reaction (eq 2).

The fluorescence spectra are convolutions of AcH^+* fluorescence generated by excited-state proton transfer (eq 2) and fluorescence resulting from direct excitation of AcH^+. This is because of the difference between pK_a and pK_a* and the large fluorescence quantum yield of AcH^+*. Fluorescence of AcH^+*

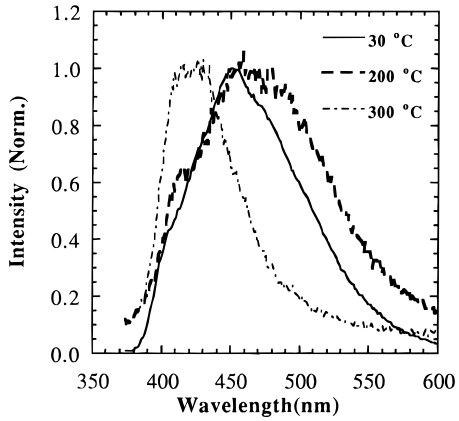

Figure 8. Steady-state fluorescence spectra of a deaerated neutral solution of acridine (1×10^{-5} M) at 3500 psia and three temperatures: 30, 200, and 300 °C. The maximum fluorescence of each spectrum is normalized to one.

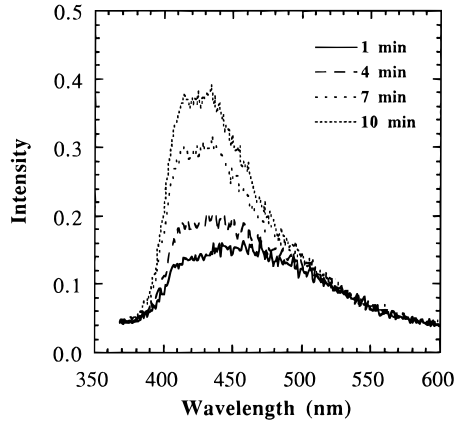

Figure 9. Steady-state fluorescence spectra of a deaerated neutral aqueous acridine solution at 250 °C and 3500 psia. The first spectrum was recorded immediately after flushing the cell and allowing one minute for the temperature and pressure to stabilize. Subsequent spectra were recorded at three minute intervals.

deriving from direct excitation of AcH^+ is significant compared to that resulting from excited-state proton transfer even when the AcH^+ concentration is much less than the Ac concentration because of the large quantum yield for fluorescence of AcH^+*. For example, at pH 8 the ground-state equilibrium favors Ac almost exclusively, but time-resolved fluorescence measurements revealed a slow growth of AcH^+* fluorescence resulting from excited-state proton transfer superimposed on a detector-limited growth of AcH^+* from direct excitation of AcH^+. The relative fluorescence intensities from AcH^+* and Ac* do not only reflect the temperature-dependent changes in the excited-state equilibrium (eq 2) exclusively but also reflect changes in the ground-state equilibrium induced by temperature (eq 3). This observation is in contrast to a previous study of excited-state proton-transfer reactions of acridine which found no evidence of direct AcH^+ excitation in pH 8 solutions of acridine.[37]

Steady-state fluorescence is a more sensitive probe of acridine decomposition than absorption measurements. A permanent fluorescence peak at about 420 nm attributable to a decomposition product grows in over time at temperatures above 200 °C (Figure 9), even though there is no detectable change in the absorption spectrum under the same conditions. Immediately after flushing the cell with new solution (allowing 1−2 min for temperature equilibration at 250 °C) fluorescence from both Ac* and AcH^+* is observed. Additional fluorescence spectra obtained in 3 min intervals reveal the growth of a decomposition product in the same spectral region as Ac*. At temperatures higher than 250 °C, the decomposition is faster. Thus, the fluorescence near 420 nm is a convolution of Ac* fluorescence and the fluorescence of a decomposition product. Neutral acridine solutions were stable in stainless steel batch reactors and analyzed by GC, and the absorption spectrum did not change over time at any temperature; however, a new absorption peak attributed to a decomposition product grew in at 380 nm in pH 3 acridine solutions above 350 °C. Fluorescence excitation spectra obtained by monitoring the 420 nm emission in neutral acridine solutions at 250 °C show the same decomposition product peak as that observed in the absorption spectra of acidic acridine solutions above 350 °C. No decomposition product absorption is observed in excitation spectra monitoring the 550 nm emission because the decomposition product does not fluoresce at this wavelength.

Acridine decomposition at high temperatures severely limits the use of steady-state fluorescence to study its excited-state equilibrium behavior because the decomposition product fluorescence overlaps the fluorescence of unprotonated acridine and is significant even in neutral water. The decomposition product absorption peak does not appear in neutral water at any temperature studied. This indicates that absorption is much less sensitive to the effects of decomposition, enabling a study of the ground-state equilibrium to 380 °C. While a decomposition product absorption peak appears in acidic solutions above 350 °C, the decomposition rate is slow enough that absorption spectra can be acquired before there are any significant spectral changes. Above 380 °C, the spectral changes caused by decomposition occur too fast to acquire emission spectra and inhibit the study of the ground-state equilibrium above this temperature. All fluorescence experiments reported here were stable over the time window of the experiment.

Huh and co-workers[33] report neutral solutions of acridine to be stable to 250 °C, but Lee and co-workers have studied acridine oxidation to (9,10*H*)-acridone at 200 °C in acidic solutions. They suggested the mechanism is autoxidation by oxygen with titanium dioxide on the cell surface acting as a catalyst.

Hydrogen-Bonding Interactions. The fluorescence intensities and lifetimes of nitrogen heterocycles are known to be sensitive to solute−solvent hydrogen-bond interactions.[38] For example, isoquinoline and acridine fluoresce much more strongly in protic solvents than in hydrocarbon solvents.[38] The traditional explanation for these observations is that the lowest excited singlet state for many nitrogen heterocycles is of n,π* character in hydrocarbon solvents but of π,π* character in alcohols and other hydrogen-bond donors, and the n,π* state is nonfluorescent because of efficient intersystem crossing and/or internal conversion.[38] State inversion is thus caused by hydrogen-bond interactions between the lone electron pair on the nitrogen and protic solvents. An n−π* excitation decreases the electron density on the nitrogen and weakens the hydrogen bonding between the excited n,π* state and the protic solvent molecules. Thus, the ground state is better solvated by protic solvents than the S_1 state (Figure 10). In an aprotic solvent, the ground state is less well solvated than the excited state and changes in the hydrogen-bond donor properties of solvents generally do not strongly influence the energies of the $\pi-\pi$* transitions. Therefore, the S_1 state of a nitrogen heterocycle may be n,π* in hydrocarbon solvents while S_2 is π,π*, but the S_1 state is π,π* and the S_2 state is n,π* in protic solvents.

Clearly this picture is a simplification. While the labels "n,π*" and "π,π*" are commonly used, it is not strictly correct to consider these as isolated electronic states. The S_1 and S_2 states are of intermediate character because of vibronic coupling;

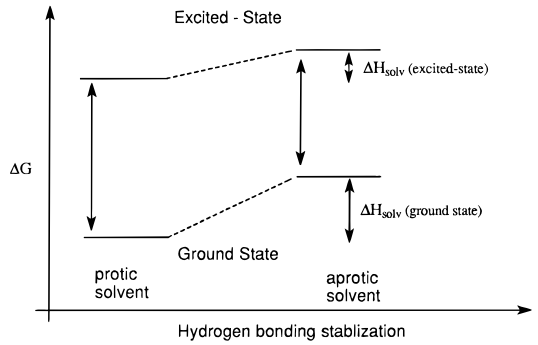

Figure 10. Effect of hydrogen bonding on the n-π^* transition energy typical of nitrogen containing heterocycles such as acridine. In protic solvents, hydrogen bonding between the solvent and the lone electron pair on the nitrogen preferentially solvates the ground state of acridine relative to the excited state because the electron density on the nitrogen is reduced in the n-π^* state, and hydrogen bonding is less stabilizing in the excited state.

that is, the states are mixed.[38,39] Vibronic coupling between the n,π^* and π,π^* states can have a profound influence on both the fluorescence intensity and lifetime of nitrogen heterocycles. For example, an analogous state inversion does not occur in isoquinoline, where the S_1 state is predominantly π,π^* in all solvents. Although the intersystem crossing quantum yield is approximately the same in both protic and aprotic solvents, isoquinoline fluoresces much less strongly in hydrocarbon solvents.

Lim and co-workers have proposed a "proximity effect" which facilitates internal conversion to explain these observations.[38,40] Although state inversion does not occur in isoquinoline, the frequency of the n,π^* transition is, nonetheless, decreased in aprotic solvents, and there is a smaller energy gap between the n,π^* and π,π^* states. This increases vibronic coupling further mixing the S_1 and S_2 states, so that the n,π^* character of the S_1 state increases. The vibronic coupling occurs through the out-of-plane vibrations of the S_1 state which are good acceptor modes for a large energy gap transition such as S_1-S_0 internal conversion.[40] Therefore, internal conversion is facilitated in aprotic solvents by the proximity effect, thus inhibiting fluorescence.

Changes in the S_1 state character also manifest themselves by a change in the fluorescence lifetime. Both acridine and isoquinoline have larger fluorescence lifetimes in protic solvents than in hydrocarbon solvents.[38,39] This is consistent with the larger fluorescence quantum yield in protic solvents. In hydrocarbon solvents, the nonradiative relaxation rate is very fast, and the S_1 state lifetime is short compared to the purely radiative relaxation rate.

The rate constants for fluorescence of acridine at pH 12, $k_f = 1/\tau$ (where $k_f = k_{nr} + k_r$) are measured at several temperatures at 3500 psia by single-photon counting (Figure 11). At this pH, only Ac is present in the ground state, and no excited-state proton transfer to Ac* occurs (Scheme 1). Thus, excitation of Ac to Ac* produces only Ac* fluorescence with a lifetime determined by k_f. The radiative rate constant is generally assumed to be temperature independent,[13,41] so the observed decrease in the fluorescence lifetime with temperature must reflect the temperature dependence of the nonradiative rate constant, k_{nr}. The fluorescence rate constants show nonlinear Arrhenius behavior (Figure 11). Lim and co-workers[40] studied the temperature dependence of fluorescence of another nitrogen-containing heterocycle, isoquinoline. Their results are also nonlinear when plotted in Arrhenius fashion (Figure 11). They concluded that this strong temperature dependence of the isoquinoline decay rate is the result of changes in hydrogen-

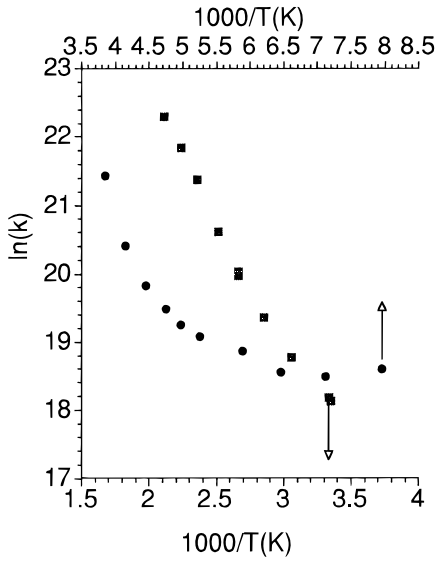

Figure 11. Temperature dependence of the 410 nm fluorescence decay rate constant (squares) at 3500 psia of acridine solutions (1×10^{-4} M) adjusted to pH 12. The previously reported temperature dependence of the fluorescence decay rate constants of isoquinoline in ethanol (circles) are shown for comparison.[40] The experimental uncertainty is ± 0.2 natural log units.

bond interactions; especially near the melting temperature of ethanol where the change was most dramatic. As the hydrogen bonds weaken, the n,$\pi^*-\pi,\pi^*$ energy gap decreases (proximity effect), and the S_1 state becomes more mixed which facilitates internal conversion to the S_0 state and decreases the fluorescence lifetime and intensity.

Arrhenius plots of fluorescence decay rates are expected to be linear with temperature in the absence of substantial solvent changes and are not generally strongly temperature or pressure dependent.[13,41] By analogy to the isoquinoline data, the curvature of our acridine data suggests a substantial change in the hydrogen-bond interactions of water above 100 °C, where the data are approximately linear between 100 and 200 °C. Above 200 °C, the fluorescence lifetime and intensity were too small to measure accurately with our equipment. Below 100 °C, the fluorescence decay rate is less temperature dependent than the data above 100 °C. Although the temperature dependence of acridine fluorescence at low temperature is weaker than at high temperature, it is still much more strongly dependent on temperature than the fluorescence lifetime and intensity of 2-naphthol.[13] Again, this suggests that hydrogen bonding influences acridine fluorescence even at low temperatures.

The temperature dependence of the absorption spectrum of acridine also suggests a change in the character of the hydrogen-bonding interactions above 100 °C. As the temperature is increased, the absorption maximum of a pH 9.2 aqueous acridine solution at 3500 psia at 355 nm shifts about 4 nm to the red, and the extinction coefficient decreases by a factor of ~1.8 (Figure 12). There is no evidence of acridine decomposition in basic solutions. Such a large change in the extinction coefficient with temperature is unusual. For example, the extinction coefficient of the 2-naphthol $\pi\rightarrow\pi^*$ absorption is independent of temperature up to 400 °C.[9] The unusual temperature dependence of the acridine extinction coefficient has been observed previously by Huh and co-workers up to 250 °C.[33] Solvent-dependent changes in the extinction coefficient have been observed with other N-heterocycles, and they were attributed to changes in local hydrogen bonding.[42]

The temperature dependence of the acridine extinction coefficient may be rationalized by considering the variability

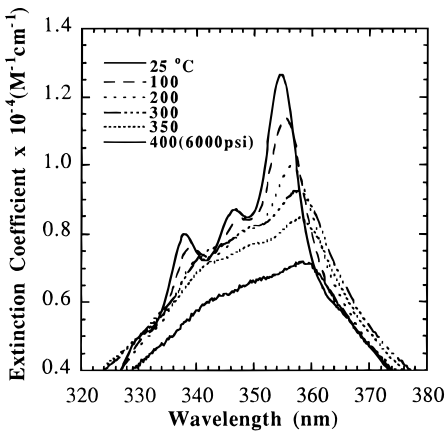

Figure 12. Absorption spectra of an aqueous acridine solution (1×10^{-4} M) adjusted to pH 9.2 at several temperatures and 3500 psia.

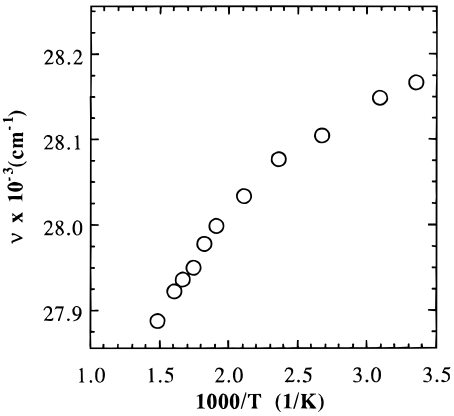

Figure 13. Temperature dependence of the frequency of maximum absorption (ν_{max}) of a solution of acridine (1×10^{-4} M) adjusted to pH 9.2 at 3500 psia. The experimental uncertainty is ± 50 cm^{-1}.

of the S_1 state character with temperature. In ambient water, the S_1 state is primarily π,π^* because hydrogen bonding preferentially stabilizes the n,π^* ground state. At elevated temperatures where hydrogen bonding dissipates, however, the contribution of n,π^* character to the S_1 state increases. Typically, n$\rightarrow\pi^*$ absorptions are at least 100 times less intense than $\pi\rightarrow\pi^*$ absorptions in the same molecule.[38,42] So, as the n,π^* character of the S_1 state increases, the $S_0\rightarrow S_1$ transition becomes weaker because of the increased coupling between the allowed π,π^* and the forbidden n,π^* transitions. The small red-shift of the absorption maximum in Figure 12 is likely due to the red-shifted S_2 transition which is expected to become stronger as its π,π^* character increases. Attempts to model the spectral behavior by deconvoluting the spectra in Figure 12 into the vibrational components of the n,π^* and π,π^* absorptions were unsuccessful because of the virtually complete overlap of the two electronic transitions and the poor resolution of the vibrational structure in the transition.

The temperature dependence of the absorption frequency of the spectra shown in Figure 12 show two nearly linear regions: from ambient temperature to ~150 °C, and above 200 °C (Figure 13). As with the fluorescence data, the abrupt change in the slope which occurs between 100 and 200 °C also suggests a marked change in the hydrogen-bond interactions in this temperature range. The absorption frequency shift with temperature is a less sensitive probe of hydrogen-bond changes than is the fluorescence lifetime because the background changes somewhat during data collection and the vibrational components of the absorption broaden.

Conclusions

The large change in water's dielectric constant on going from subcritical to supercritical conditions has a profound effect on the thermodynamics of acridine protonation. In subcritical water, the protonation reaction is exothermic because the proton is a much stronger acid than the acridinium cation. Near the critical point, the relative solvation of the acridinium cation and the proton undergo large changes with temperature at constant pressure. As water's dielectric constant decreases with temperature, solvation favors the acridinium cation because of its smaller charge-to-volume ratio and drives the equilibrium toward the protonated species (endothermic behavior). At constant density where the dielectric constant is relatively constant, the reaction remains exothermic at all conditions studied.

Both acridine absorption and fluorescence are sensitive to hydrogen-bonding interactions between water and the lone electron pair on the nitrogen in acridine. Changes in the absorption spectrum, extinction coefficient, and fluorescence lifetime with increasing temperature are consistent with the changes observed on going from a protic to an aprotic solvent. These indicate that hydrogen-bonding interactions decrease in water as the temperature is increased. A relatively rapid change observed between 100 and 200 °C is consistent with the predictions of molecular dynamics simulation.[29]

Acknowledgment. This work was supported by a University Research Initiative (30374-CH-URI) and AASERT Grant DAAH 04-93-6-0363 of the Army Research Office and by the Separations Research Program at the University of Texas.

References and Notes

(1) Vinaogradov, S. N.; Linnell, R. H. *Hydrogen Bonding*; Van Nostrand Reinhold Co.: New York, 1971.
(2) White, H. J.; Sengers, J. V.; Neumann, D. B.; Bellows, J. C. *Physical Chemistry of Aqueous Systems*; Begell House: New York, 1995.
(3) Franks, F., Ed. *Water: A Comprehensive Treatise*; Plenum Press: New York, 1972; Vol. 1.
(4) (a) Boock, L. T.; Klein, M. T. *Ind. Eng. Chem. Res.* **1994**, *33*, 2554. (b) Savage, P. E.; Gopalan, S.; Mizan, T. I.; Martino, C. J.; Brock, E. E. *AIChE J.* **1995**, *41*, 1723.
(5) Brennecke, J. *ACS Symp. Ser.* **1993**, *514*, 122.
(6) Gloyna, E. F.; Lee, L. *Waste Management* **1993**, *13*, 379.
(7) Shaw, R. W.; Brill, T. B.; Clifford, A. A.; Eckert, C. A.; Franck, E. U. *Chem. Eng. News* **1991**, *69*, 26.
(8) Tester, J. W.; Holgate, H. R.; Armellini, F. J.; Webley, P. A.; Killilea, W. R.; Hong, G. T.; Barnes, H. E. *ACS Symp. Ser.* **1993**, *518*, 35.
(9) Xiang, T.; Johnston, K. P. *J. Phys. Chem.* **1994**, *98*, 7915.
(10) Xiang, T.; Johnston, K. P. *J. Solut. Chem.*, submitted.
(11) Balbuena, P. B.; Johnston, K. P.; Rossky, P. J. *J. Phys. Chem.* **1996**, *100*, 2716.
(12) Bennett, G. E.; Balbuena, P. B.; Johnston, K. P.; Rossky, P. J. *J. Am. Chem. Soc.* **1996**, *118*, 6746.
(13) Green, S.; Xiang, T.; Johnston, K. P.; Fox, M. A. *J. Phys. Chem.* **1995**, *99*, 13787.
(14) O'Connor, D. V.; Phillips, D. *Time Correlated Single Photon Counting*; Academic Press: New York, 1984; Chapter 4.
(15) Birks, J. B. *Photophysics of Aromatic Molecules*; John Wiley and Sons: New York, 1970; p 123.
(16) Budavari, S., Ed. *The Merck Index*, 11th ed.; Merck & Co., Inc.: Rahway, NJ, 1989.
(17) Cummings, P. T.; Cochran, H. D.; Simonson, J. M.; Mesmer, R. E.; Karaborni, S. *J. Chem. Phys.* **1991**, *94*, 5606.
(18) Cui, S. T.; Harris, J. G. *J. Phys. Chem.* **1995**, *99*, 2900.
(19) Balbuena, P. B.; Johnston, K. P.; Rossky, P. J. *J. Am. Chem. Soc.* **1994**, *116*, 2698.
(20) Balbuena, P. B.; Johnston, K. P.; Rossky, P. J. *J. Phys. Chem.* **1995**, *99*, 1554.
(21) Flanagin, L. W.; Balbuena, P. B.; Johnston, K. P.; Rossky, P. J. *J. Phys. Chem.* **1995**, *99*, 5196.
(22) Balbuena, P. B.; Johnston, K. P.; Rossky, P. J. *J. Phys. Chem.* **1996**, *100*, 2706.
(23) Sitkoff, D.; Sharp, K. A.; Honig, B. *J. Phys. Chem.* **1994**, *98*, 1978.
(24) Bennett, G. E.; Rossky, P. J.; Johnston, K. P. *J. Phys. Chem.* **1995**, *99*, 16136.

(25) Robinson, G. W.; Thistlewaite, P. J.; Lee, J. *J. Phys. Chem.* **1986**, *90*, 4224.
(26) Lee, J.; Robinson, G. W.; Bassez, M.-P. *J. Am. Chem. Soc.* **1986**, *108*, 7477.
(27) Lee, J.; Griffin, R. D.; Robinson, G. W. *J. Chem. Phys.* **1985**, *82*, 4920.
(28) Ryan, E. T.; Xiang, T.; Johnston, K. P.; Fox, M. A. *J. Phys. Chem.* **1996**, *100*, 9395.
(29) Guissani, Y.; Guillot, B. *J. Chem. Phys.* **1993**, *98*, 8221.
(30) Gorbaty, Y. E.; Kalinichev, A. G. *J. Phys. Chem.* **1995**, *99*, 5336.
(31) Ireland, J. F.; Wyatt, P. A. H. *Adv. Phys. Org. Chem.* **1976**, *12*, 131.
(32) Mesmer, R. E.; Marshall, W. L.; Palmer, D. A.; Simoson, J. M.; Holmes, H. F. *J. Solut. Chem.* **1988**, *17*, 699.
(33) Huh, Y.; Lee, J.; McPhail, D. C.; Kim, K. *J. Solut. Chem.* **1993**, *22*, 651.
(34) Tester, J. W.; Holgate, H. R.; Armellini, F. J.; Webley, P. A.; Killilea, W. R.; Hong, G. T.; Barner, H. E. In *Emerging Technologies in Hazardous Waste Management III*; American Chemical Society: Washington, DC, 1993; p 35.
(35) Uematsu, M.; Franck, E. U. *J. Phys. Chem. Ref. Data.* **1980**, *9*, 1291.
(36) Haar, L.; Gallagher, J. S.; Kell, G. S. *NBS/NRC Steam Tables*; Hemisphere: Washington, DC, 1984.
(37) Gafni, A.; Brand, L. *Chem. Phys. Lett.* **1978**, *58*, 346.
(38) Wehry, E. L. In *Practical Fluorescence*; Guilbault, G. G., Ed.; Marcel Dekker, Inc.: New York, 1990.
(39) Diverdi, L. A.; Topp, M. R. *J. Phys. Chem.* **1984**, *88*, 3447.
(40) Madej, S. L.; Okajima, S.; Lim, E. C. *J. Chem. Phys.* **1976**, *65*, 1219.
(41) Claude, J. P.; Meyer, T. J. *J. Phys. Chem.* **1995**, *99*, 51.
(42) Rao, C. N. R. *Ultra-Violet and Visible Spectroscopy*; Butterworth: London, 1961.